Received September 30, 2021, accepted October 12, 2021, date of publication October 19, 2021, date of current version October 28, 2021.

Digital Object Identifier 10.1109/ACCESS.2021.3121494

Adaptive Cruise Control With Gain Scheduling Technique Under Varying Vehicle Mass

MUHAMMAD RONY HIDAYATULLAH AND JYH-CHING JUANG, (Member, IEEE)
Department of Electrical Engineering, National Cheng Kung University, Tainan 70101, Taiwan
Corresponding author: Muhammad Rony Hidayatullah (n28087010@gs.ncku.edu.tw)

This work was supported by the Ministry of Science and Technology (MOST), Taiwan, under Grant MOST 110-2218-E-006-026.

ABSTRACT Today, advanced driver-assistance systems (ADAS) come up with different abilities. One of them is the adaptive cruise control (ACC) system. The ACC system is a continuation of research on cruise control (CC) system, which integrates spacing control with the existing velocity control on the CC system. The vehicles with an ACC system guarantee traffic safety while at the same time ensure a well-driving sense. Many studies have demonstrated numerous control techniques applied as ACC controllers to accomplish uncertainty and perturbation issues. Nevertheless, most of the existing papers assumed the model vehicle dynamics as a linear time-invariant (LTI) system while designing the ACC controller. This paper proposed an ACC controller using the gain scheduling technique to deal with the model vehicle dynamics as a linear parameter varying (LPV) system. The passenger vehicle's mass varies during ACC operation depending on how many passengers or loads on the vehicle's trunks. Later, the vehicle's mass is estimated by recursive least square (RLS) with a forgetting factor. Then, the disk margin is utilized to provide the high-level robustness at each operating or ''frozen'' point. The robustness performance will be analyzed using the worst-case gain metric while the uncertainty is modeled by integral quadratic constraints (IQC). The LPV system behavior, such as the rate vehicle's mass, is also considered in the analysis. The effectiveness algorithm is validated through joint simulation between Matlab/Simulink and PreScan. The last, the comparison performance between gain scheduling and fixed gain ACC controller is evaluated.

INDEX TERMS Adaptive cruise control, advanced driver assistance systems, cruise control, gain scheduling controller, linear parameter varying system, spacing control.

NOMENCLATURE

$B_{r,\max}$	Maximum brake pressure.
$T_{h,\max}$	Maximum throttle.
m, $\hat{m}$	Actual and estimated mass of the vehicle.
δ_{safe}, δ_{rel}, δ_0	Safe distance, relative distance, and minimum distance between vehicles.
v_{ref} , $v_{x,h}$	Longitudinal reference velocity and actual of velocity of host vehicle.
t_g	Time gap between vehicles.
X_a	Position of target or other vehicles in front of the host vehicle.
X_h	Position of the host vehicle.
e_{vc}, e_{sc}	Error velocity and error distance.
u, χ	Control signal and rate of control signal.
$\underline{u}$, $\bar{u}$	Lower and upper boundary of the control signal.
$\underline{\chi}$, $\bar{\chi}$	Lower and upper boundary of the control signal rate.
$(\bullet)_{vc}$, $(\bullet)_{sc}$	Subscripts *vc* and *sc* defined velocity control and spacing control mode.

The associate editor coordinating the review of this manuscript and approving it for publication was Michail Makridis.

I. INTRODUCTION

The expeditious technology development of advanced driver-assistance systems (ADAS) delivers the driverless vehicle to be a reality. The society of automotive engineers (SAE) separated the level automation of ADAS to be five levels [1]. At level 4 or 5, ADAS is expected to diminish or even abolish traffic accidents on the road and offers new versatility for society, such as safe driving, pleasant driving sense, and

This work is licensed under a Creative Commons Attribution 4.0 License. For more information, see https://creativecommons.org/licenses/by/4.0/

saving time travel [2]–[6]. Based on [7], [8], ADAS has three subsystems: perception, planning, and control. The control subsystem is responsible for delivering a proper command for throttle, brake, and steering to render the vehicle follow the reference trajectory set by the user or driver. It defines how the vehicle will interact and behave with the surrounding environment. Therefore, the control subsystem ultimately performs an indispensable role, albeit it cannot work in a solitary subsystem. Nevertheless, the perception and planning become worthless if the controller fails to follow the reference trajectory [8]. The control system architecture in the ADAS is apportioned into longitudinal and lateral control [9]. In this work, we concentrated on longitudinal control.

The major problem of longitudinal control is split into two parts: what type of longitudinal dynamics and control strategy need to be used [6]. The longitudinal dynamics are referred to the mathematic equation of vehicle models such as kinematic, linear dynamics, or nonlinear dynamics. At the same time, control strategies are frequently chosen to depend on the vehicle model considered and the uncertainties are faced. The early stage of longitudinal control applications is cruise control (CC), where the vehicle will follow the velocity command by the driver. Later on, adaptive cruise control (ACC) come up with a new feature to preserve the distance between the vehicles at a proper safe distance and maintain the vehicle velocity within the velocity command at the same time.

Currently, there are a bunch of existing works that concern on ACC controller. Wang *et al.* designed non-singular terminal sliding mode control (NTSMC) with radial basis function (RBF) to handle the nonlinear vehicle dynamics under less accurate model vehicle dynamics and able to reduce the chattering effect [10]. The other works using RBF-based controller with amplitude saturation controller (ASC) is proposed by [11] where the RBF-based controller will replace the ASC task as a controller with a smooth transition after several online learning. Their subsequent work proposed a deep belief network semi-supervised controller-based (DBNSSC) also succeed to replace the main controller after several online learning [12]. Lin and Görges presented a robust MPC (RMPC) as ACC controller with two steps design the controller: a linear feedback control is designed offline, and an online optimization is solved each time with different models to decouple the performance and robustness [13]. Another work using MPC framework as ACC controller is proposed in [14]–[18] to achieve fuel efficiency, comfort, and safety on ACC mode. Jiang *et al.* presented an ACC control law called a linear exponential-of-quadratic Gaussian (LEQG) with risk-sensitive parameters that rendered six-vehicle behaviors and two control modes (expensive and inexpensive control mode) [19]. Liberis *et al.* proposed the predictor-based with integral action to guarantee stability, zero steady-state, string stability, and non-negative impulse response for ACC feedback controller to handle actuator and sensor delay [20]. In the following works, their utilized a partial derivative equation (PDE) as ACC controller, and the Aw-Rascle-Zhang-type (ARZ-type) model is considered as traffic flow model [21]. The proposed method succeeded in achieving performance metrics such as fuel consumption, total travel time, and comfort.

Furthermore, various spacing policies are formulated in order to achieve road efficiency with ACC system. Wu *et al.* presented a survey of different kinds of ACC spacing policies and found that all these spacing policies failed to ensure stability (internal stability, string stability, and traffic flow stability), safety, and comfort at the same time [22]. Therefore, a trade-off between stability, safety, and comfort are required. Yang *et al.* proposed variable time gaps between vehicles to improve the vehicle safety and driving experience when deceleration in emergency conditions [23]. Besides road efficiency, several existing works focused on energy consumption. Chen *et al.* proposed model-free and real-time ecological ACC (eco-ACC) based on action-dependent heuristic dynamic programming (ADHDP) controller to accomplish safety, comfortable driving, improve long-life battery, and energy consumption for car-following scenario [24]. The other works of eco-ACC with objective energy consumption applications are presented in [25]–[32].

Further, to enhance the ACC system, Dang *et al.* integrated the ACC and lane-change systems (LCACC) with considering the risk of lane change analysis and performed in driver-in-loop [33]. Xu *et al.* integrated ACC with lane-keeping (LK) by utilizing control barrier functions (CBFs) [34]. Another work combined ACC system and collision avoidance (CA) presented in [35] and [36]. Plessen *et al.* performed ACC system with obstacle avoidance (OA) using a combination of linear time-varying MPC and geometry corridor planning to allow the vehicle to perform with four driving modes: ACC, obstacle avoidance (multiple static and dynamic objects), obstacle-free road tracking, and emergency braking [37]. Cheng *et al.* integrated an ACC system with direct yaw moment control (DYC) to guarantee driving experience while driving on a curved road [38].

In addition, some work formulized ACC controller using intelligent control strategy and data-driven based. Li *et al.* used reinforcement learning (RL) algorithms to solve the drift counteraction optimal control (DCOC) problem in order to find optimal control law for ACC system with multiple constraints such as safety, comfort, and fuel economy [39]. The other works using RL on ACC controller are given in [26] and [40]. Another work using learning-based methods such as recurrent neural networks (RNN) to handle interference vehicles during cut-in is presented in [41]. Chen *et al.* analyzed the trade-off ACC system such as safety, comfort, and traffic efficiency based on large amounts of real road data and it bring a guide for engineers to set the ACC parameters based on a data-driven method [42]. The other work using data-driven on ACC are presented by [43], [44].

After a conscientious literature review, a critical issue is missed from the attention worthy of ameliorating for ACC systems, which are listed in the following.

(1) All work reviewed earlier, on the ACC system, assumed the model vehicle dynamics is a linear time-invariant (LTI) system, which is a severe flaw. The model vehicle dynamics are linear parameter varying (LPV) systems. This issue is unexplored during the development of longitudinal vehicle controllers.
(2) Several existing works are considering the LPV system on the ADAS applications using gain scheduling controller published in journals and conferences. Even so, the objective of the concerns of the existing work on velocity tracking [45]–[47], trajectory tracking [6], [48], 49], and spacing policy [50]. Need to be underlined, if we address the ACC controller, then we design the controller that has two modes, namely velocity and distance tracking not only velocity tracking.
(3) Most of the existing works considered scheduled variable as linear and angular velocity [6], [48], control signal saturation [45], vehicle's velocity and road grade [46], [47], [49], and time gap [50]. None of all existing works are considering the vehicle's mass as scheduled variable. The vehicle's mass changed during operation depend on how many passengers or loads are on the vehicle and is worthy of further investigation.
(4) Some existing work lacks robustness analysis and often analyzes the robustness system at each operating or ''frozen'' point based on the analysis LTI system. It missed apprehending LPV system behavior [51], [52].

Concerning the above problems, this paper *proposes the ACC system using a gain scheduling controller for the LPV system, where the mass of vehicles varied during ACC operation and provides robustness analysis and LPV system's performance*. Need to be highlighted, this paper focused on the passenger vehicles type with the ACC system. Consequently, the purpose is not always to achieve a small distance between vehicles, and also, not all passenger vehicles will move in the platoon. The proportional-derivative with low-pass filter (PD) gain scheduling is selected as the ACC controller strategy and tuned based on the linear model vehicle dynamics at the frozen points. The linear model vehicle dynamics is attained by using system identification. The primary contribution of this paper compared with the existing works is summarized as follows.

(1) The ACC system based on gain scheduling controller for LPV system is proposed for both control modes in ACC system, namely velocity and distance tracking.
(2) Unlike the existing work, in this paper, the varying parameter or scheduling variable is the vehicle's mass. The mass of passenger vehicles will vary during operation depends on how many passengers are inside the vehicle and the loads in the vehicle's trunk.
(3) The disk margin is applied instead of classical gain and phase margins to provide a high level of robustness at each frozen point. The robustness analysis must be carried out since the controller gains are tuned based on linear model vehicle dynamics at the frozen points, while in the simulation, we applied a highly nonlinear model vehicle dynamics provided by PreScan. Then, the worst-case gain metric is adopted to examine the robust performance of the LPV system, where the uncertainty is registered by integral quadratic constraints (IQC).

TABLE 1. TIS sensor specifications.

Parameters	TIS 1	TIS 2	Unit
Range	30	150	Meter
Time sampling	25	25	Hertz
Elevation beam angle	9	9	Degree
Azimuth beam angle	80	9	Degree
Maximum detection object	32	32	-

The remaining section of the paper is organized in this manner. Section II addresses the problem formulation of this paper. Section III discusses the LPV system. The gain scheduling controller and robustness analysis used in this paper are explained in Section IV. Section V presented the robustness analysis and simulation results. The conclusion is given in Section VI.

II. PROBLEM FORMULATION

In this section, the vehicle dynamics are explained. Next, the sensor specifications and performance are presented. Then, the low-level controller architecture is shown. After that, the proposed upper-level controller is explained. The last, the control objectives are given.

A. VEHICLE DYNAMICS

The simulation is done by incorporating Matlab/Simulink and PreScan. PreScan provided the nonlinear vehicle dynamics that consisted of engine, transmission, chassis, shift logic, and switch between automatic and manual shift. The simulation architecture is shown in Figure 1. In this work, the SUV with seven seats is chosen as a vehicle with an ACC system.

B. SENSING

In this paper, two technology-independent sensors (TIS) are equipped on the vehicle, which then has different range works, one for long-range and the others for short-range. In PreScan, TIS is proposed to validate and verify the active scanning sensor such as radar, lidar, and other laser scan sensors [53]. Hence, TIS operated with the same principles such as radar and lidar. Table 1 shows the TIS sensor specifications. The range of sensors is commonly selected as regard of the ACC applications. Figure 2 shows the performance of the TIS sensor. The longitudinal range error is getting smaller when the object gets closer since the noise on range measurement is multiplicative.

C. LOW-LEVEL CONTROLLER

The low-level controller (LLC) converted the desired acceleration from the upper-level controller (ULC) into throttle or

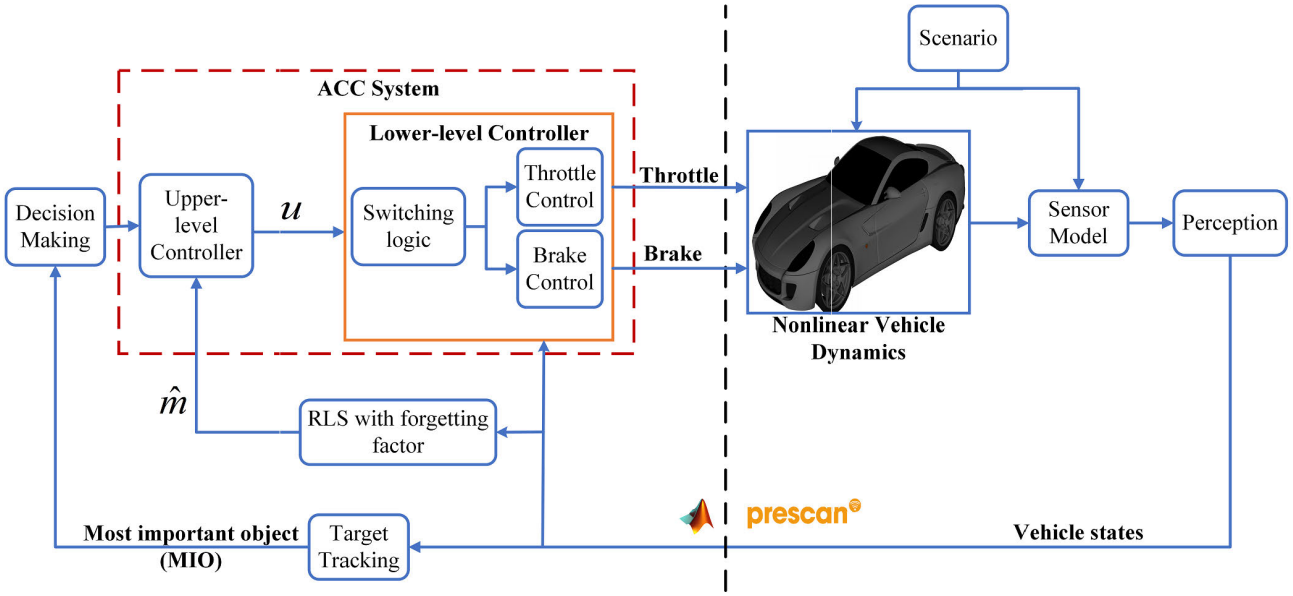

FIGURE 1. Simulation architecture.

brake. It consists of switching logic, a throttle controller, and a braking controller. Figure 3 show the architecture of LLC. The detail of the LLC and its performance can be seen in [54].

D. UPPER-LEVEL CONTROLLER

In the ACC system, the ULC has two controller modes: velocity control and spacing control. Most of the paper used fixed controller gains on both velocity and spacing controllers. Fixed controller gains are effective to deal with the LTI system. Despite that, it has inadequately performance to deal with the LPV system. The detail regarding the LPV system can be referred to Section III. In this paper, we used the gain scheduling controller to deal with LPV system, as shown in Figure 4. As a result, the controller gains on the velocity and spacing controllers changed based on the scheduled variable, namely the vehicle's mass. The vehicle's mass is estimated by RLS with a forgetting factor. The lookup table of the controller gains block has consisted of controller gains obtained in offline. When the vehicle's mass is changed, then the controller gains will be updated by this block. The velocity and spacing controllers generated the control signals, namely desired acceleration. The switching logic selected those control signals to deliver to the LLC. The switching logic in ULC will determine which vehicle mode either CC or ACC.

E. CONTROL OBJECTIVES

The longitudinal controller objectives are divided into the ULC and LLC objectives. The ULC should be met in the following condition.

1) PERFORMANCE

In ACC, the vehicle should be able to maintain the safe distance as defined in (1) while at the same time also maintain the velocity to stay within the user or driver limit as defined in (2).

$$\delta_{safe}(t) = \delta_0 + t_g v_{x,h}(t) \tag{1}$$

$$\lim_{t\to\infty} \left| e_{vc}(t) \; = v_{ref}(t) - v_{x,h}(t) \right| \triangleq 0 \tag{2}$$

2) COLLISION AVOIDANCE

When the preceding vehicle stopped, then the distance between host and preceding vehicle is non-negative such as defined by,

$$\delta_{rel}(t) = X_a(t) - X_h(t) \geq \delta_0 \tag{3}$$

3) ASYMPTOTIC TIME GAP SYNCHRONIZATION

The safe distance in (1) is depending on time gap and velocity of the vehicle. At steady state condition, it should be satisfied with the below condition.

$$\lim_{t\to\infty} \left| e_{sc}(t) = \delta_{safe}(t) - \delta_{rel}(t) \right| \triangleq 0 \tag{4}$$

4) COMFORT

The great driving experience is crucial in passenger vehicle. Therefore, the ULC should be designed by following the below constraints.

$$u(t) \in \left[\underline{u}(t), \bar{u}(t)\right], \underline{u}(t) \leq \bar{u}(t) \tag{5}$$

$$\chi(t) \in \left[\underline{\chi}(t), \bar{\chi}(t)\right], \underline{\chi}(t) \leq \bar{\chi}(t) \tag{6}$$

The LLC objective is to identify whichever vehicle must apply the throttle and brake. After that, the desired acceleration from ULC will convert to throttle or brake pedal position.

Remark 1: The relative distance and relative velocity between vehicles can be measured using TIS. The actual velocity of the vehicle can be measured accurately by the

wheel-speed sensor, such as odometry. The actual acceleration of the vehicle can be obtained from the acceleration sensor. The minimum distance is set as big as $\delta_0 = 5$ meters.

Remark 2: Referred to (5) and (6), the vehicle system exhibited nonlinearity. Further, in PreScan, several dead zones are applied in the actuator of the vehicle dynamics. Those problems can degrade the controller performance, especially if our controller has integral terms. Nevertheless, those issues are out of the scope of this work. The readers are invited to read recent publications to handle those issues using fuzzy structure to avoid offline identification and identify the dead zones parameter in [55] to improve controller performance under actuator dead zones.

III. LINEAR PARAMETER VARYING SYSTEM

Given a nonlinear system that shown as follows,

$$\begin{aligned} \dot{x} &= f(x, u) \\ y &= g(x, u) \end{aligned} \tag{7}$$

where $x \in \mathbb{R}^{n_x}$, $u \in \mathbb{R}^{n_u}$, and $y \in \mathbb{R}^{n_y}$ are the state, input, and output of the system. Let ϑ and $\dot{\vartheta}$ are defined as the unknown time-varying parameters and its rate that assumed lied on hyperrectangle, $\vartheta, \dot{\vartheta} \in \mathbb{R}^{n_\vartheta}$, $n_\vartheta \geq n_u$. n_x, n_u, n_y, and n_ϑ are the set of strictly positive integer members, $n_x, n_u, n_y, n_\vartheta \in \mathbb{Z}_+^*$. Eventually, the scheduled parameter, ϑ, should be able to measure, or an estimation technique is necessary to perform. In practice, the estimated value consisted of the error part, as shown in the following.

$$\begin{aligned} \hat{\vartheta}_i(t) &= \vartheta_i(t) + \upsilon_i(t), \quad \forall i \in \{1, 2, \ldots, n_\vartheta\} \\ \hat{\dot{\vartheta}}_i(t) &= \dot{\vartheta}_i(t) + \dot{\upsilon}_i(t), \quad \forall i \in \{1, 2, \ldots, n_\vartheta\} \end{aligned} \tag{8}$$

where $\upsilon(t), \dot{\upsilon}(t) \in \mathbb{R}^{n_\vartheta}$ is the error or uncertain part. We supposed that $\upsilon(t)$ and $\dot{\upsilon}(t)$ are small so that $\hat{\vartheta}_i(t) \triangleq \vartheta_i(t)$. However, several case must be considered $\upsilon(t)$ and $\dot{\upsilon}(t)$ as done by [56]. After that, the equation (7) can be written as nonlinear parameter varying (NPV) system as follows,

$$\begin{aligned} \dot{x} &= f(x, u, \vartheta(t)) \\ y &= g(x, u, \vartheta(t)) \end{aligned} \tag{9}$$

Need to be highlighted, the parameter $\dot{\vartheta}$ implicitly influenced the NPV system in (9).

The LPV system has a linear form system and has a certain range value of ϑ that change over time during the operation depends on $\dot{\vartheta}$. Therefore, the equation (9) can be transformed to the LPV system with $x(0) = 0$ as follows,

$$\begin{aligned} \dot{x}(t) &= A(\vartheta(t))\, x(t) + B(\vartheta(t))\, u(t) \\ y(t) &= C(\vartheta(t))\, x(t) + D(\vartheta(t))\, u(t) \end{aligned} \tag{10}$$

Also, the equation (10) can be written as,

$$G(\vartheta(t)) = \frac{y(t)}{u(t)} = \left[\begin{array}{c|c} A(\vartheta(t)) & B(\vartheta(t)) \\ \hline C(\vartheta(t)) & D(\vartheta(t)) \end{array}\right] \tag{11}$$

where the matrices $A \in \mathbb{R}^{n_x \times n_x}$, $B \in \mathbb{R}^{n_x \times n_u}$, $C \in \mathbb{R}^{n_y \times n_x}$, and $D \in \mathbb{R}^{n_y \times n_u}$ are a function of $\vartheta(t)$ then the model becomes the time-varying. For the affine case,

$$\begin{aligned} \{\bullet\} &= \{A_0, B_0, C_0, D_0\} + \{A_1, B_1, C_1, D_1\}\, \vartheta_1(t) \\ &\quad + \{A_2, B_2, C_2, D_2\}\, \vartheta_2(t) + \cdots + \left\{A_p, B_p, C_p, D_p\right\} \vartheta_p(t) \\ \{\bullet\} &\in \left\{ \begin{array}{l} \{A_0, B_0, C_0, D_0\} + \\ \sum_{i=1}^{p} \{A_i, B_i, C_i, D_i\}\, \hat{\vartheta}_i(t),\ \sum_{i=1}^{p} \vartheta_i(t) = 1,\ \vartheta_i(t) \geq 0 \end{array} \right\} \end{aligned} \tag{12}$$

where $\{\bullet\}$ refers to $\{\bullet\} = \{A(\vartheta(t)), B(\vartheta(t)), C(\vartheta(t)), D(\vartheta(t))\}$ and $p = 2^{n_\vartheta}$ is the constructed hyperrectangle with 2^{n_ϑ} vertexes and n_ϑ number of scheduling parameters. Several existing works proposed trapezoidal polytope, triangle polytope, and two-vertices to reduce the conservatism in LPV system [57]. The domain of interest is defined as a compact domain, Ω, where the $\vartheta(t)$ and $\dot{\vartheta}(t)$ are well defined, then we have,

$$\begin{aligned} \vartheta_k(t) \in \Omega_1 &= \left\{\vartheta_k(t) \in \left[\vartheta_{lb,k}, \vartheta_{ub,k}\right], \forall k \in \{1, 2, \ldots, n_\vartheta\}\right\} \\ \dot{\vartheta}_k(t) \in \Omega_2 &= \left\{\dot{\vartheta}_k(t) \in \left[\dot{\vartheta}_{lb,k}, \dot{\vartheta}_{ub,k}\right], \forall k \in \{1, 2, \ldots, n_\vartheta\}\right\} \end{aligned} \tag{13}$$

where $\vartheta_{lb} \leq \vartheta_{ub}$ and $\dot{\vartheta}_{lb} \leq \dot{\vartheta}_{ub}$ are defined as the lower and upper bound of $\vartheta(t)$ and $\dot{\vartheta}(t)$.

The performance of LPV system can be assessed by induced L_2 norm. For a given finite energy to the input signals that satisfies $\forall \vartheta(t) \in \Omega_1$, the induced L_2 norm calculates the maximum gain or the largest amplification of the LPV system.

Definition 1: Induced L_2 norm.

Defined $\|y\|_2 = \sqrt{\int_0^\infty y^T(t) y(t) dt}$ and $\|u\|_2 = \sqrt{\int_0^\infty u^T(t) u(t) dt}$. Moreover, u is bounded signals, $u \in L_2$, that satisfies $\|u\|_2 < \infty$. The induced L_2 norm of the system in (11) is defined as,

$$\|G(\vartheta(t))\|_2 = \sup_{u \neq 0, u \in L_2, \vartheta \in \Omega_1, x(0)=0} \frac{\|y\|_2}{\|u\|_2} \tag{14}$$

The induced L_2 norm required the ''quadratic storage function'' to provide the sufficient condition to upper bound of the induced L_2 norm gain of the system in (11). The sufficient condition is given in term of LMIs in Lemma 1.

Lemma 1 [58]: Bounded real lemma or Kalman–Yakubovich–Popov lemma.

Suppose $A(\vartheta(t))$ is Hurwitz and the system $G(\vartheta(t))$ satisfies with conditions $\forall \vartheta(t) \in \Omega_1$ and $\forall \dot{\vartheta}(t) \in \Omega_2$. The system in (11) is exponentially stable and $\|G(\vartheta(t))\|_\infty \leq \varepsilon$ if and only if hold the following condition.

$$\begin{aligned} &P(\vartheta(t)) = P(\vartheta(t))^T > 0 \\ &\begin{bmatrix} (\bullet) & P(\vartheta(t))\, B(\vartheta(t)) \\ B(\vartheta(t))^T P(\vartheta(t)) & -\varepsilon I \end{bmatrix} + \frac{1}{\varepsilon} \begin{bmatrix} C(\vartheta(t))^T \\ D(\vartheta(t))^T \end{bmatrix} \begin{bmatrix} C(\vartheta(t)) & D(\vartheta(t)) \end{bmatrix} < 0 \end{aligned} \tag{15}$$

where $(\bullet) = A(\vartheta(t))^T P(\vartheta(t)) + P(\vartheta(t)) A(\vartheta(t)) + \partial P\left(\vartheta(t), \dot{\vartheta}(t)\right)$ and ε is a positive real number. The $\partial P\left(\vartheta(t), \dot{\vartheta}(t)\right)$ is defined as follows,

$$\partial P\left(\vartheta(t), \dot{\vartheta}(t)\right) = \sum_{i=1}^{n_\vartheta} \frac{\partial P(\vartheta(t))}{\partial \vartheta_i(t)} \dot{\vartheta}_i(t) \tag{16}$$

The proof of equation (15) can be seen in [58].

IV. GAIN SCHEDULING CONTROLLER

In this section, we will explain the gain scheduling which is used for ULC. Then, the robustness analysis for LPV systems will be presented.

A. PROPORTIONAL-DERIVATIVE GAIN SCHEDULING

The design process of the gain scheduling controller is shown in the following.

1. Given a bounded domain of interest, we determined several frozen points to cover it.
2. We performed the linearizing technique of the nonlinear systems at each frozen point.
3. We tuned the controller gain at each frozen point.
4. We designed the gain scheduling architecture by ensuring a smooth transition between each gain.

The output feedback control law for system (10) can be defined as,

$$u(t) = K(\vartheta(t)) C(\vartheta(t)) x(t) \tag{17}$$

where

$$\begin{aligned} K(\vartheta(t)) &= K_0 + K_1\vartheta_1(t) + K_2\vartheta_2(t) + \cdots + K_p\vartheta_p(t) \\ K(\vartheta(t)) &\in \left\{ K_0 + \sum_{i=1}^{p} K_i\vartheta_i(t), \sum_{i=1}^{p} \vartheta_i(t) = 1, \vartheta_i(t) \geq 0 \right\} \end{aligned} \tag{18}$$

K is the output feedback gain matrix. The closed-loop system can be obtained from (10) and (17) as follows,

$$\dot{x}(t) = A_{cl}(\vartheta(t)) x(t) \tag{19}$$

where

$$\begin{aligned} A_{cl}(\vartheta(t)) &= A_{cl,0} + A_{cl,1}\vartheta_1(t) + A_{cl,2}\vartheta_2(t) \\ &+ \cdots + A_{cl,p}\vartheta_p(t) \\ A_{cl,i}(\vartheta(t)) &= A_i(\vartheta(t)) + B_i(\vartheta(t)) K(\vartheta(t)) C(\vartheta(t)) \\ A_{cl}(\vartheta(t)) &\in \left\{ A_{cl,0} + \sum_{i=1}^{p} A_{cl,i}\vartheta_i(t), \sum_{i=1}^{p} \vartheta_i(t) = 1, \vartheta_i(t) \geq 0 \right\} \end{aligned} \tag{20}$$

Consider the PD as the control algorithm, then equation (17) can be written as follows,

$$u(t) = k_p(\vartheta(t)) e(t) + k_d(\vartheta(t)) \dot{e}(t) \tag{21}$$

For the sake of comprehensibility, the equation (21) can be rewritten in the following.

$$u(t) = k_p(\vartheta(t)) y(t) + k_d(\vartheta(t)) \dot{y}(t) \tag{22}$$

If $y(t) = C(\vartheta(t)) x(t)$ and the equation (22) can be written as follows,

$$u(t) = k_p(\vartheta(t)) C(\vartheta(t)) x(t) + k_d(\vartheta(t)) C(\vartheta(t)) \dot{x}(t) \tag{23}$$

From (19) and (22), the closed-loop systems with PD controller is given by,

$$\begin{aligned} \dot{x}(t) = &\left[A(\vartheta(t)) + B(\vartheta(t)) k_p(\vartheta(t)) C(\vartheta(t))\right] x(t) \\ &+ B(\vartheta(t)) k_d(\vartheta(t)) C(\vartheta(t)) \dot{x}(t) \end{aligned} \tag{24}$$

The equation (24) can be written in compact form as follows,

$$\Theta(\vartheta(t)) \dot{x}(t) = A_{cl}(\vartheta(t)) x(t) \text{ or } \dot{x}(t) = A_{cld}(\vartheta(t)) x(t) \tag{25}$$

where

$$\begin{aligned} A_{cld}(\vartheta(t)) &= \Theta(\vartheta(t))^{-1} A_{cl}(\vartheta(t)), \\ \Theta(\vartheta(t)) &= I - B(\vartheta(t)) k_d(\vartheta(t)) C(\vartheta(t)), \text{ and} \\ A_{cl}(\vartheta(t)) &= A(\vartheta(t)) + B(\vartheta(t)) k_p(\vartheta(t)) C(\vartheta(t)). \end{aligned}$$

Remark 3: The closed-loop stability is not affected by the reference signal so the reference signal is assumed to be in (22).

In this paper, the scheduled variable is represented by the mass of the vehicle as shown in the following.

$$\vartheta(t) = m(t) \tag{26}$$

The mass of the passenger vehicle frequently changed depend on the passengers and loads. Therefore, the mass of the vehicle should be correctly estimated. We followed work from [59], [60] that have been done to solve the vehicle's mass estimation issue.

B. DISK MARGIN

The robustness is crucial to consider when designing the controller because we cannot perfectly model the actual vehicle. The vehicle has an exceptionally complex nonlinear system, decreased performance year by year, and manufactured process variation. The tragic reality is, we tuned the controller gain based on the model that has uncertainty. As a result, the controller has poor performance and risk of instability. Figure 5 shows the interconnection between the nominal system and uncertainty on the LTI system. The disk margin is introduced by [51], [61] to answer the classical gain and phase margins limitation. It can capture the perturbation on both gain and phase that coincided in the system. The disk margin defined the system's margin as a disk in the complex plane, as shown in Figure 6a. The whole blue region is the stable region, including the nominal system and uncertainty in gain and phase variation. The Δ is defined as follows,

$$\Delta \in S(\alpha_{\max}, \delta) = \frac{1 + \alpha_{\max}\frac{1-\delta}{2}}{1 - \alpha_{\max}\frac{1+\delta}{2}} \tag{27}$$

The equation (27) is under the assumption $\left|\alpha_{\max}\frac{1-\delta}{2}\right| < 1$. The term of $\Delta \in S(\alpha_{\max}, \delta)$ mean that Δ lied on the area of set $S(\alpha_{\max}, \delta)$. Afterwards, disk center and radius are calculated as follows,

$$c_{disk} = \frac{\gamma_{\max} + \gamma_{\min}}{2}, r_{disk} = \frac{\gamma_{\max} - \gamma_{\min}}{2} \tag{28}$$

The maximum and minimum intercept points on real axis of the disk is defined as the maximum and minimum gain margins and can be calculated as follows,

$$\gamma_{\max} = \frac{2 + \alpha_{\max}(1-\delta)}{2 - \alpha_{\max}(1+\delta)}, \gamma_{\min} = \frac{2 - \alpha_{\max}(1-\delta)}{2 + \alpha_{\max}(1+\delta)} \tag{29}$$

Moreover, the maximum and the minimum phase margin can be obtained by,

$$\begin{aligned} \phi_{\max} &= \begin{cases} \cos^{-1}\left(\frac{1+\gamma_{\max}\gamma_{\min}}{\gamma_{\max}+\gamma_{\min}}\right), & \text{for } r_{disk} \le c_{disk} \\ +\infty, & \text{for otherwise} \end{cases} \\ \phi_{\min} &= -\phi_{\max} \end{aligned} \tag{30}$$

In the case of $\phi_{\max} = +\infty$, it means that the feedback system is stable for any phase variation.

Lemma 2 [61]: Disk margin condition.

Suppose the δ is skew parameter of the disk margin and the closed loop of the nominal system is stable then the disk margin is shown as,

$$\alpha_{\max} = \left\| T(s) + \frac{\delta - 1}{2} \right\|_{\infty}^{-1} \tag{31}$$

where $T(s)$ is defined as sensitivity function of the system in Figure 6b. The proof of equation (31) can be seemingly seen in [61].

Definition 2: Supposed Δ is LTI system and lied on the set $S(\alpha_{\max}, \delta)$ such that $\Delta \in S(\alpha_{\max}, \delta)$. By using small gain theorem, the closed loop system will stable for all $\|\Delta\|_{\infty} < \kappa_{DM}$ and $\kappa_{DM} = \frac{\alpha_{\max}}{2}$ when balanced case $\delta = 0$.

The equations (29) and (30) are expressed only for the safe area of gain or phase variation. It is related to the classical gain and phase margins. The connection between the gain and phase variations can be computed by,

$$\phi = \cos^{-1}\left(\frac{\gamma^2 + \gamma_{\max}\gamma_{\min}}{\gamma(\gamma_{\max} + \gamma_{\min})}\right) \tag{32}$$

where $\phi \in [\phi_{\min}, \phi_{\max}]$ is the phase variation for a certain value of $\gamma \in [\gamma_{\min}, \gamma_{\max}]$. Moreover, the safe area of the set $\Delta \in S(\alpha_{\max}, \delta)$ can be rewritten as,

$$\Delta \in S(\alpha_{\max}, \delta) = \frac{1 + \alpha_{\max} e^{i\theta_{disk}} \frac{1-\delta}{2}}{1 - \alpha_{\max} e^{i\theta_{disk}} \frac{1+\delta}{2}} \tag{33}$$

where $\theta_{disk} \in [0, \pi]$. The parameter δ controlled the different amount of the gain variation where positive value will give more gain variation and otherwise. The parameter $\alpha_{\max}$ controlled the size of disk and determined how large the gain and phase variation that can be tolerated.

Remark 4: The disk margin is more conservative than the classical gain and phase margin. However, it provided a high level of robustness. As the authors of this paper, we believe that the system such as aircraft and autonomous vehicle requires a high level of robustness analysis. Hence, that is the background of our stance to use disk margin instead of classical gain and phase margin.

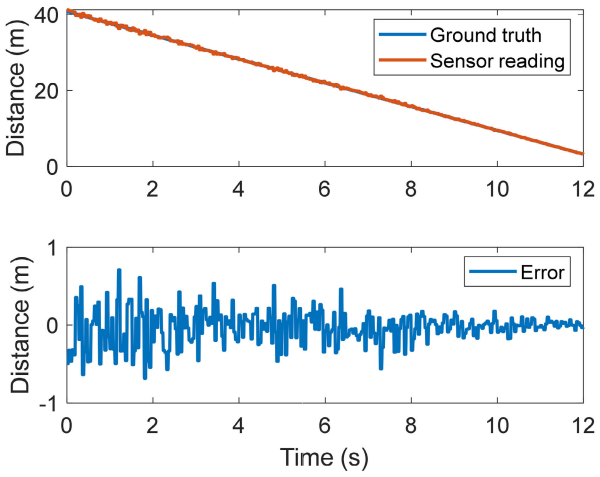

FIGURE 2. TIS performance on the longitudinal range measurement.

C. WORST CASE GAIN

The G in the Figure 5 change to be $G(\vartheta(t))$ due to LPV system as shown in Figure 7. The dynamics interconnection in Figure 7 can be written as follows,

$$\begin{aligned} \frac{d}{dt}\begin{bmatrix} x_G(t) \\ x_\psi(t) \end{bmatrix} &= A(\vartheta(t))x(t) + B_1(\vartheta(t))w(t) + B_2(\vartheta(t))u(t) \\ z(t) &= C_1(\vartheta(t))x(t) + D_{11}(\vartheta(t))w(t) \\ &\quad + D_{12}(\vartheta(t))u(t) \\ y(t) &= C_2(\vartheta(t))x(t) + D_{21}(\vartheta(t))w(t) \\ &\quad + D_{22}(\vartheta(t))u(t) \end{aligned} \tag{34}$$

The Δ is assumed LTI system and satisfies the IQC where Δ is defined by (Ψ, M), $\Delta \in (\Psi, M)$. Figure 7 show that the input and output signals of Δ are filtered by stable linear system Ψ. If $\Delta \in (\Psi, M)$ then the signal z respects the below constraint for $T \ge 0$,

$$\int_0^T z(t)^T M z(t) dt \ge 0 \tag{35}$$

The dashed block of Δ in Figure 7 indicated that Δ will not be included for the analysis. Let $w = \Delta v$ is assumed as external signal that subject to the constraint on signal z as shown in (35). Since is LTI system then it follows $F(s)\Delta(s) = \Delta(s)F(s)$ where $F(s)$ is any stable system. Due to $w = \Delta v$ then $Fw = \Delta Fv$ and signal z is defined as follows,

$$z = \Psi\begin{bmatrix} v \\ w \end{bmatrix} = \begin{bmatrix} F & 0 \\ 0 & F \end{bmatrix}\begin{bmatrix} v \\ w \end{bmatrix} \tag{36}$$

Definition 3 [51]: Suppose Δ is LTI system and defined by IQC such that $\Delta \in (\Psi, M)$. Moreover, the symmetric matrix is given by $M = \begin{bmatrix} \kappa_{IQC}^2 & 0 \\ 0 & -1 \end{bmatrix}$ and Ψ is defined by (36) then Δ satisfies for (35) and $\|\Delta\|_\infty < \kappa_{IQC}$.

Lemma 3 [52]: Extended bounded real lemma.

Supposed the system in (34) is written in term of $F_u(G(\vartheta(t)), \Delta)$ and be well posed. Let Δ be an LTI where $\Delta \in (\Psi, M)$. Then, the upper bounded worst-case gain of $\|F_u(G(\vartheta(t)), \Delta)\|_\infty \leq \varepsilon_{IQC}$ if and only if satisfies with the following condition.

$$
\begin{aligned}
&P(\vartheta(t)) = P(\vartheta(t))^T > 0, \lambda > 0 \\
&\begin{bmatrix} (\bullet) & P(\vartheta(t)) B_1(\vartheta(t)) & P(\vartheta(t)) B_2(\vartheta(t)) \\ B_1(\vartheta(t))^T P(\vartheta(t)) & 0 & 0 \\ B_2(\vartheta(t))^T P(\vartheta(t)) & 0 & -\varepsilon_{IQC} I \end{bmatrix} \\
&+\lambda \begin{bmatrix} C_1(\vartheta(t))^T \\ D_{11}(\vartheta(t))^T \\ D_{12}(\vartheta(t))^T \end{bmatrix} M \begin{bmatrix} C_1(\vartheta(t)) & D_{11}(\vartheta(t)) & D_{12}(\vartheta(t)) \end{bmatrix} \\
&+\frac{1}{\varepsilon_{IQC}} \begin{bmatrix} C_2(\vartheta(t))^T \\ D_{21}(\vartheta(t))^T \\ D_{22}(\vartheta(t))^T \end{bmatrix} \begin{bmatrix} C_2(\vartheta(t)) & D_{21}(\vartheta(t)) & D_{22}(\vartheta(t)) \end{bmatrix} \\
&< 0
\end{aligned} \tag{37}
$$

where $(\bullet) = A(\vartheta(t))^T P(\vartheta(t)) + P(\vartheta(t)) A(\vartheta(t)) + \partial P\left(\vartheta(t), \dot{\vartheta}(t)\right)$ and ε_{IQC} is a positive real number. The $A(\vartheta(t))$ is Hurwitz and the system $G(\vartheta(t))$ satisfies with conditions $\forall \vartheta(t) \in \Omega_1$ and $\forall \dot{\vartheta}(t) \in \Omega_2$. The proof of equation (37) can be seen in [52]. Therefore, the robustness analysis for LPV system required to find the variables $P(\vartheta(t)) = P(\vartheta(t))^T > 0$, $\lambda > 0$, and $\varepsilon_{IQC} < \infty$ that lead the Lemma 3 feasible.

Remark 5: Lemma 3 is an extended version of Lemma 1, which delivers the advantage that the worst-case gain metric is able to analyze the robust performance under uncertain conditions on the LPV system. As a result, we utilized Lemma 1 to analyze the nominal system and Lemma 3 to analyze the system with uncertainty.

V. SIMULATION AND DISCUSSION

A. IDENTIFICATION

The vehicle type is SUV with seven seats. The linear model vehicle dynamics at each frozen point is obtained by System identification toolbox in Matlab. The vehicle's mass varied from 1820 kg (without passenger or nominal mass) to 3120 kg (with full load) during operation. These values are called the extreme frozen point representing the lowest and highest vehicle's mass during operation. Then, we have three regions condition, as shown in Table 2. The identification can be done with the following steps:

Step 1: We collected the input and output data. In this work, the input data is desired acceleration, $a_{x,des}$, and the output data is the actual acceleration of the vehicles, a_x.

Step 2: The relation between input and output data are approximated by the linear first-order model that exposed in transfer function as shown in (38).

$$\frac{a_x(s)}{a_{x,des}(s)} = \frac{k_G(\vartheta(t))}{1 + \tau_G(\vartheta(t))\, s} \tag{38}$$

Step 3: We used *System identification toolbox* to obtain the parameters k_G and τ_G. After we completed for vehicle's mass 1820 kg, we repeated from *Step 1* to obtain the parameters for vehicle's mass 3120 kg.

Figure 8 shows the comparison between actual and model response with step input at the extreme frozen point. The model is acquired from identification fit with the actual response as big as 84.47% and 82.49%.

From (4) and (38), the state space form of LPV system can be rendered as follows,

$$
\begin{aligned}
\begin{bmatrix} \dot{a}_x(t) \\ \dot{v}_x(t) \\ \dot{\delta}_0 \end{bmatrix} &= \begin{bmatrix} -\tau_G^{-1}(\vartheta(t)) & 0 & 0 \\ 1 & 0 & 0 \\ t_g & 1 & 0 \end{bmatrix} \begin{bmatrix} a_x(t) \\ v_x(t) \\ \delta_0 \end{bmatrix} \\
&+ \begin{bmatrix} \tau_G^{-1}(\vartheta(t)) \\ 0 \\ 0 \end{bmatrix} u(t-\theta) \\
\begin{bmatrix} v_x(t) \\ \delta_0 \end{bmatrix} &= \begin{bmatrix} 0 & k_G(\vartheta(t)) & 0 \\ 0 & 0 & k_G(\vartheta(t)) \end{bmatrix} \begin{bmatrix} a_x(t) \\ v_x(t) \\ \delta_0 \end{bmatrix}
\end{aligned} \tag{39}
$$

where $u(t) = a_{x,des}$ and the transmission delay between ULC and LLC, θ, is accurately modelled by the third order Padé approximation [62].

Remark 6: The value of region 2 in Table 2 lied between the region 1 and region 3.

B. PD CONTROLLER

The controller gains are tuned with the intention to fulfil the ULC objective in Section II. In addition, the ACC controller has two modes as velocity and distance tracking, which ACC control law defined as follows,

$$
\begin{aligned}
u(s) &= \min\left(u_{vc}(s), u_{sc}(s)\right) \\
u_{(\bullet)}(s) &= \left(k_{p,(\bullet)} + \frac{k_{d,(\bullet)} s}{1 + t_f s}\right) e_{(\bullet)}(s)
\end{aligned} \tag{40}
$$

The $(\bullet)$ refers to spacing control (sc) or velocity control (vc). The controller gains in (40) are obtained based on the

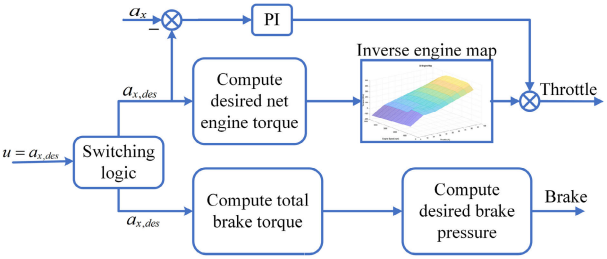

FIGURE 3. Low-level controller architecture.

TABLE 2. Vehicle work specification.

Parameters	Region 1	Region 2	Region 3
$\vartheta = m$	1820	$1820 < \vartheta < 3120$	3120
k_G	1.0371	$\frac{-2.9669}{10^4}\vartheta + 1.5771$	0.6514
τ_G	0.4156	$\frac{4.6154}{10^5}\vartheta + 0.3316$	0.4756
θ	$rand(0, 0.1)$	$rand(0, 0.1)$	$rand(0, 0.1)$
t_g	1	1	1
t_f	0.2	0.2	0.2
$k_{p,sc}$	1.5	$\frac{7.6923}{10^4}\vartheta + 0.1$	2.5
$k_{d,sc}$	2.3	$\frac{11.5385}{10^4}\vartheta + 0.2$	3.8
$k_{p,vc}$	1.3	$\frac{4.3077}{10^4}\vartheta + 0.516$	1.86
$k_{d,vc}$	0.27	$\frac{\vartheta}{10^4} + 0.088$	0.4

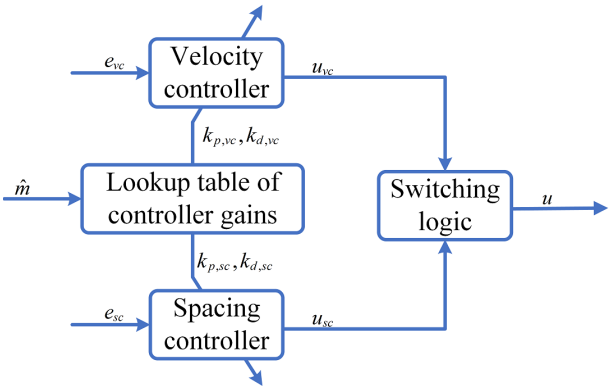

FIGURE 4. Proposed upper-level controller architecture.

linear vehicle dynamics in (39) and its values are shown in Table 2.

C. ROBUSTNESS ANALYSIS

1) DISK MARGIN

In this part, we evaluated that the controller gains in Table 2 have sufficient margins to handle the uncertainty due to the linear model from identification cannot perfectly figure out the actual vehicle behavior. The disk margin will check the stability margins at each frozen point for both ACC controller modes.

a: DISK MARGIN ON SPACING CONTROLLER

We found that the smallest disk margin for each frozen point in the domain of interest, $\forall\vartheta(t) \in \Omega_1$, occurred when the vehicle's mass is 2600 kg (region 2) as shown in Figure 9. The magnitude gain margin is 2.89 (9.23 dB) and phase margin is 51.9^o at frequency 4.7 rad/s which can handle the maximum system delay is around 0.19 seconds as shown

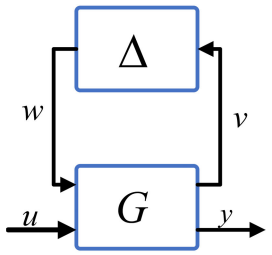

FIGURE 5. Interconnection between nominal system and uncertainty [60].

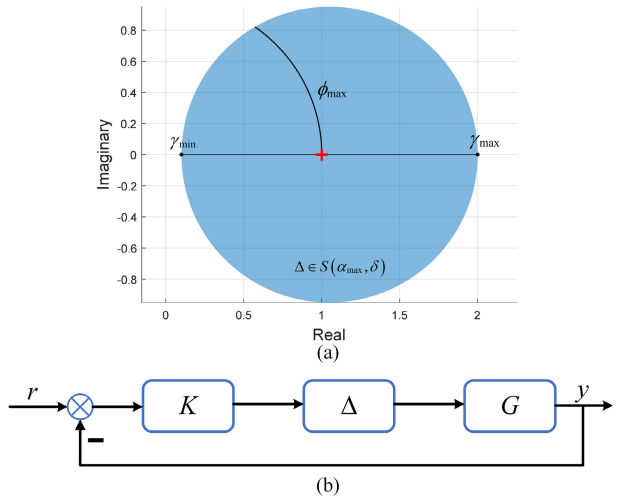

FIGURE 6. Disk margin representation.

in Figure 10. However, these values only for gain or phase variation. Figure 11 shows the range of gain and phase variations when vehicle's mass is 2600 kg. It can observe that the limit gain variation will reduce if the demand of phase variation increases as shown in Figure 11, specifically in the black marked point. Further details, when the phase variation absence then the feedback loop can handle gain variation as big as 9.23 dB. However, in the black marked point, when the phase variation is around 42.82^o then the feedback loop can only handle gain variation as big as 5.23 dB. Furthermore, based on Lemma 2 and Definition 2, we can find the smallest bound of uncertainty for each frozen point in the domain of interest, $\forall\vartheta(t) \in \Omega_1$ as big as $\kappa_{DM} = 0.4864$ so that $\|\Delta\|_\infty < 0.4864$.

b: DISK MARGIN ON VELOCITY CONTROLLER

Same as spacing controller, the smallest disk margin for each frozen point in the domain of interest, $\forall\vartheta(t) \in \Omega_1$, occurred when the vehicle's mass is 2600 kg. The gain margin is 3.3 (10.46 dB) and phase margin is 56.6^o at frequency 1.75 rad/s which can handle the maximum system delay is around 0.56 seconds. Based on Lemma 2 and Definition 2, we can find the smallest bound of uncertainty for each frozen point in the domain of interest, $\forall\vartheta(t) \in \Omega_1$, as big as $\kappa_{DM} = 0.5385$ so that $\|\Delta\|_\infty < \kappa_{DM} = 0.5385$.

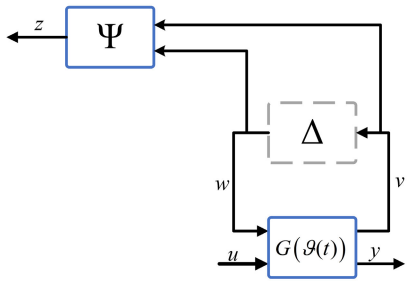

FIGURE 7. Integral quadratic constraint analysis interconnection.

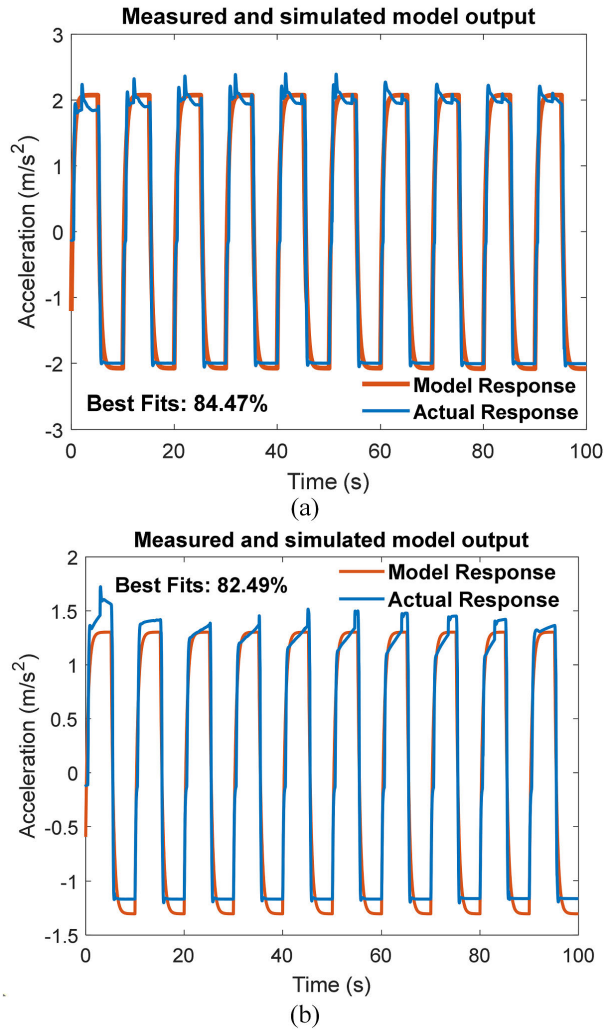

FIGURE 8. Comparison between actual and model with step input. (a) vehicle's mass 1820 kg and (b) vehicle's mass 3120 kg.

2) WORST-CASE GAIN

Even if the disk margin evaluated stability margin at each frozen point, it still could not ensure the stability margin of a complete LPV system. It is because of the disk margin analysis without considers the effect of $\dot{\vartheta}(t)$. Therefore, the worst-case gain metric with IQC will analyze and evaluate the robust performance considering the effect of $\dot{\vartheta}(t)$. As mentioned in Section IV.D, the uncertainty is represented by IQC

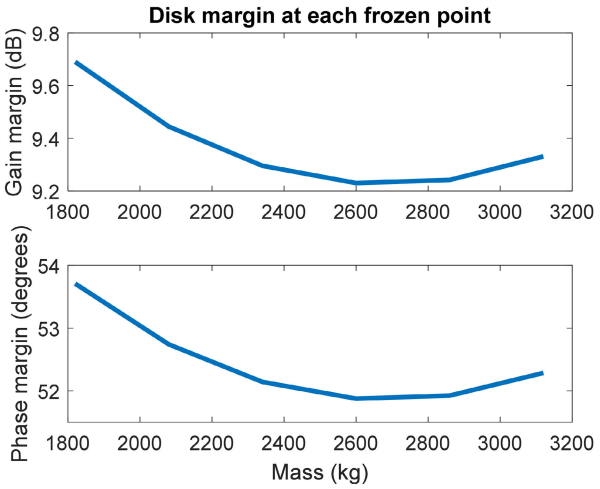

FIGURE 9. Disk margin at each frozen point.

so that $\Delta \in (\Psi, M)$ where $\Psi = I$ and M as defined in Definition 3. Same as disk margin, the worst-case gain analysis also analyzed both control modes of ACC controller.

a: WORST-CASE GAIN ON SPACING CONTROLLER

At nominal system, $\kappa_{IQC} = 0$, and $|\dot{\vartheta}(t)| \leq \infty$, the upper bound of L_2 gain is 7.4687 based on Lemma 1. Further, when $\kappa_{IQC} = 0.2$, the upper bound of worst-case gain is 10.4954 based on Lemma 3. Figure 12 shows that the upper bound of gain gradually raise up to $\kappa_{IQC} = 0.3$. When $\kappa_{IQC} > 0.36$, the feasible solution on Lemma 3 cannot be found as shown in Figure 12.

Now, we consider the rate change as big as $|\dot{\vartheta}(t)| \leq 100$ kg. First, we need to define the basis function required for bounded rate change analysis in the LPV system. There are no rules to choose the basis function despite choosing as simple as possible due to the computation loads. In this work, we examined three different basis functions as follows,

$$\begin{aligned} P_{bf1}(\vartheta(t)) &= P_0 + P_1\vartheta \\ P_{bf2}(\vartheta(t)) &= P_0 + P_1\vartheta + P_2\vartheta^2 \\ P_{bf3}(\vartheta(t)) &= P_0 + P_1\vartheta + P_2\vartheta^2 + P_3\vartheta^{-1} \end{aligned} \tag{41}$$

Figure 13 shows the upper bound of worst-case L_2 gain under $|\dot{\vartheta}(t)| \leq 100$ kg for three different basis functions. Comparing with Figure 12, the feasible solution on Lemma 3 increases up to $\kappa_{IQC} = 0.44$ for basis function 1 and basis function 2 while $\kappa_{IQC} = 0.445$ for basis function 3. We can conclude that using low- and high-order basis functions are not yielding significant improvement. For each basis function, the upper bound of L_2 gain gradually raises to $\kappa_{IQC} = 0.4$.

To analyze the effect of scheduled variable rate change, we set $\kappa_{IQC} = 0.1$, and rate change varied from 25 kg to 125 kg. Figure 14 shows the upper bound of worst-case L_2 gain for different rate changes. The upper bound of worst-case L_2 gain gets large when the rate changes increase for three different basis functions.

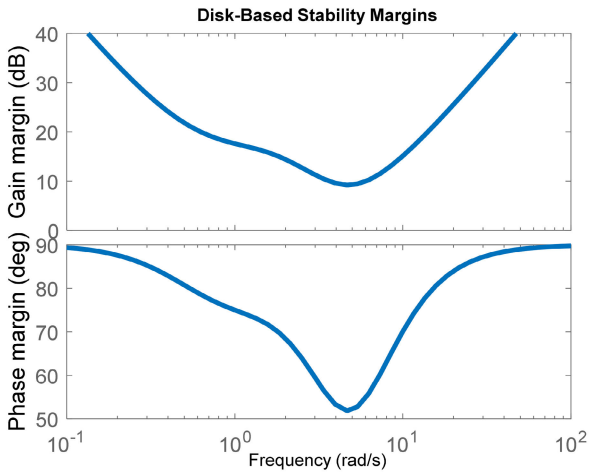

FIGURE 10. Disk margin at vehicle's mass 2600 kg.

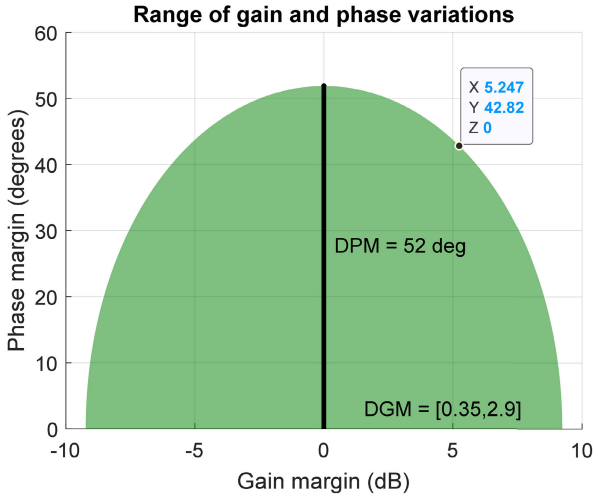

FIGURE 11. Range of gain and phase variations of disk margin.

b: WORST-CASE GAIN ON VELOCITY CONTROLLER

On velocity controller, when $\kappa_{IQC} > 0.41$, the feasible solution on Lemma 3 cannot be found for unbounded rate change,. Comparing with unbounded rate change $\left|\dot{\vartheta}(t)\right| \leq \infty$, the bounded rate change $\left|\dot{\vartheta}(t)\right| \leq 100$ kg show that the feasible solution on Lemma 3 increases up to $\kappa_{IQC} = 0.502$ for basis function 1 and basis function 2 while $\kappa_{IQC} = 0.509$ for basis function 3. Same as spacing controller, the usage of high order basis function brings a slightly different result. The upper bound of worst-case L_2 get large when the variation of the rate change is immense. It occurred for three different basis functions.

Both robustness analyses, disk margin and worst-case gain, have an upper bound of uncertainty. We can conclude that $\kappa_{IQC} < \kappa_{DM}$. Figure 12 and Figure 13 show that when the upper bound of uncertainty κ_{IQC} close to κ_{DM} then the upper bound of worst-case L_2 gain led to infinity. It is indicated by Lemma 3 that it fails to find a feasible solution.

Remark 7: In robustness analysis, the uncertainty, Δ, is modeled as multiplicative and placed in the system's input.

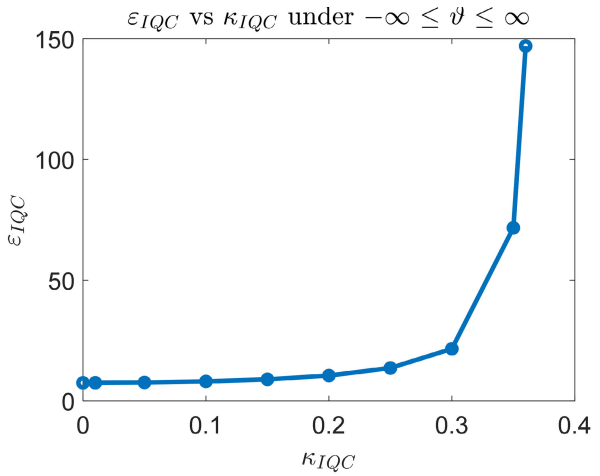

FIGURE 12. Worst-case gain under unbounded vehicle's mass rate.

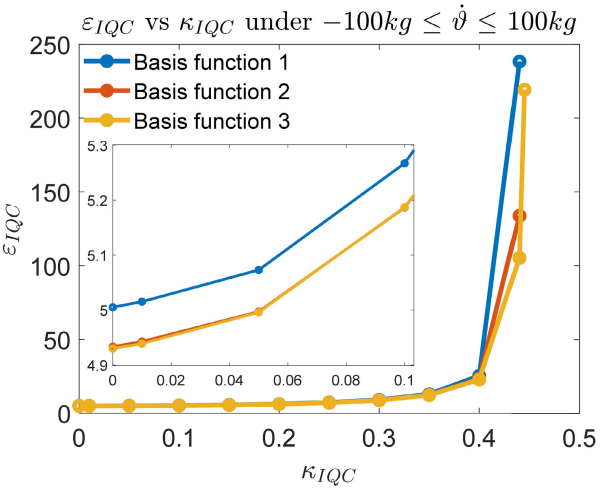

FIGURE 13. Worst-case gain with different basis function under bounded vehicle's mass rate.

D. SIMULATION

In the last step, we implemented our ACC controller through Matlab/Simulink integrated with PreScan. In this work, we assumed that the AVs operated as self-driving taxis for ride-sharing. Hence, several phases in the simulation scenario will be explained in the following.

1. In the beginning, the vehicle is empty (1820 kg) and goes to pick up the passengers.
2. After picking up the passengers, the vehicle's mass changed to 2150 kg.
3. When arrived at the passenger's destination, the vehicle's mass back to 1820 kg and goes to pick up other passengers.
4. Again, after picking up the passengers, the vehicle's mass changed to 2950 kg.
5. When arrived at the passenger's destination, the vehicle's mass back to 1820 kg and pick up other passengers.

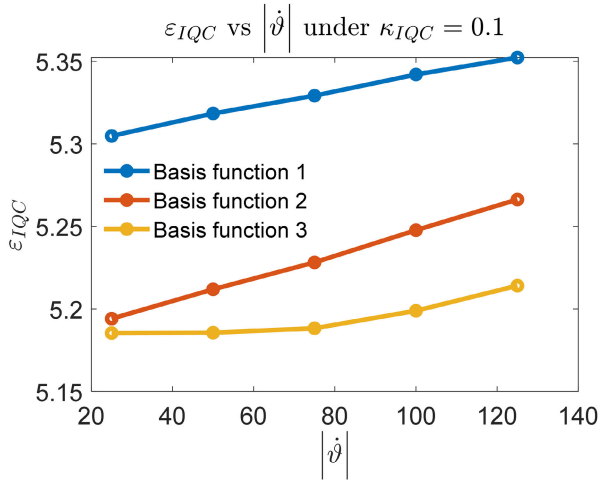

FIGURE 14. Worst-case gain with different basis function under different vehicle's mass rate.

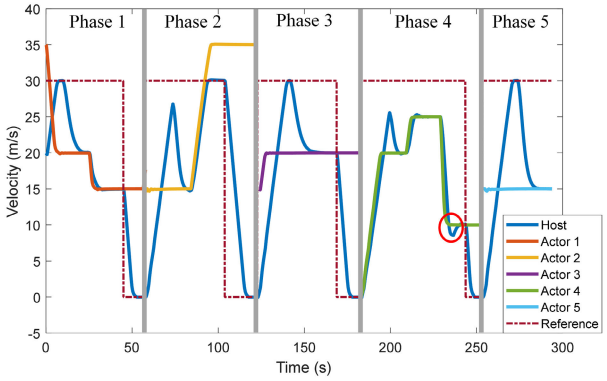

FIGURE 15. Velocity of the host vehicle using PD gain scheduling.

Table 3 shows several settings and constraints in this scenario.

TABLE 3. Simulation settings.

Parameters	Value	Unit
$B_{r,\max}$	0-150	bar
$T_{h,\max}$	0-100	%
$\underline{u}$, $\overline{u}$	-6, 2	ms^{-2}
$\underline{\chi}$, $\overline{\chi}$	-1.5, 1.5	ms^{-3}
Simulation rate	100	Hz

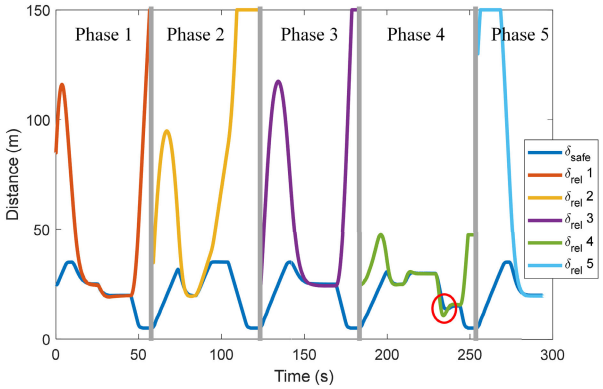

FIGURE 16. Distance tracking of the host vehicle using PD gain scheduling.

1) ACC WITH PD GAIN SCHEDULING

The results of ACC controller using PD gain scheduling are explained in the following.

a: PHASE 1

The host vehicle with an initial velocity of 20 m/s and mass of 1820 kg headed to passenger's location as shown in Figure 15. There was a vehicle, called actor 1, in front of the host vehicle with relative distance as far as 85 meters as shown in Figure 16. The legend $\delta_{rel,1}$ in Figure 16 indicated the relative distance between host vehicle and actor 1 where is calculated based on (3). Therefore, we can observe that host vehicle in the CC mode. At this mode, our controller shows a satisfy velocity tracking performance in Figure 15. It indicated with the host vehicle's velocity is able to track reference velocity. Later on, actor 1 decelerated from velocity 35 m/s to 20 m/s. At 10 seconds in Figure 15, the host vehicle changed its mode into spacing control where the host vehicle started to decelerate as a means to maintain a safe distance. At this mode, our controller objective is distance tracking which previously defined in (4). As a result, the host vehicle's velocity does not track the reference velocity anymore. We can deduce that the error velocity between reference velocity and host vehicle's velocity is getting bigger when the host vehicle changed into spacing control mode and otherwise. It is because both modes have a different objective as defined in (2) and (4). Figure 16 shows that the host vehicle is able to maintain a safe distance even if the actor 1 changed its velocity. Around 45 seconds, the host vehicle decelerated to 0 m/s due to its arrived at passenger's location and ready to carry passengers to another location.

b: PHASE 2

After picked up passengers, the vehicle's mass changed to 2150 kg. Need to be highlighted, the vehicle in front of the host vehicle changed to be actor 2. Actor 1 in phase 1 has left the host vehicle far away because the host vehicle needs to stop to pick up the passengers. At the beginning of phase 2, the host vehicle was in the spacing control mode. Then the actor 2 accelerated to its velocity 35 m/s. Figure 15 and Figure 16 show during phase 2 that the host vehicle maintains its distance during spacing control mode, and its velocity stays within the reference velocity during CC mode. At around 104 seconds, the host vehicle decelerated to 0 m/s due to its arrival at the passenger's destination and ready to pick up other passengers.

c: PHASE 3

Bear in mind, the vehicle's mass back to 1820 kg after phase 2. Similar to phase 2, the vehicle in front of the host vehicle changed to be actor 3. Actor 3 accelerated in the

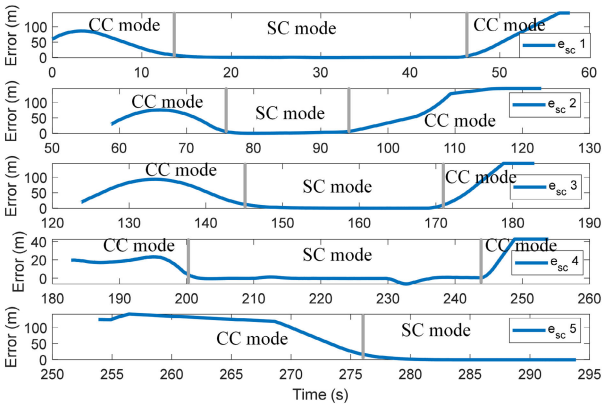

FIGURE 17. Evolution distance error of the host vehicle using PD gain scheduling.

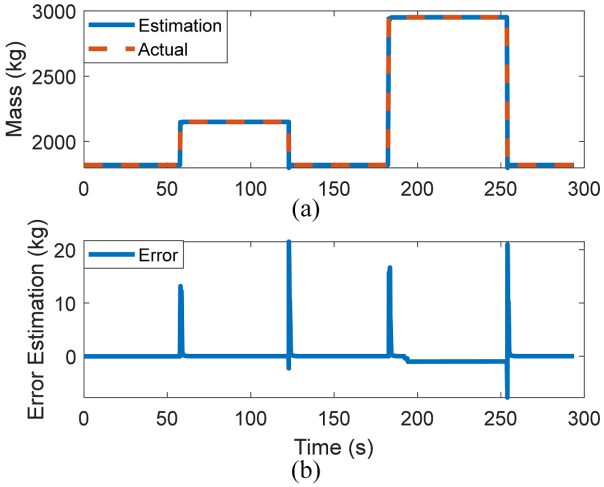

FIGURE 18. Vehicle's mass estimation performance. (a) Comparison between estimation and actual mass and (b) error estimation.

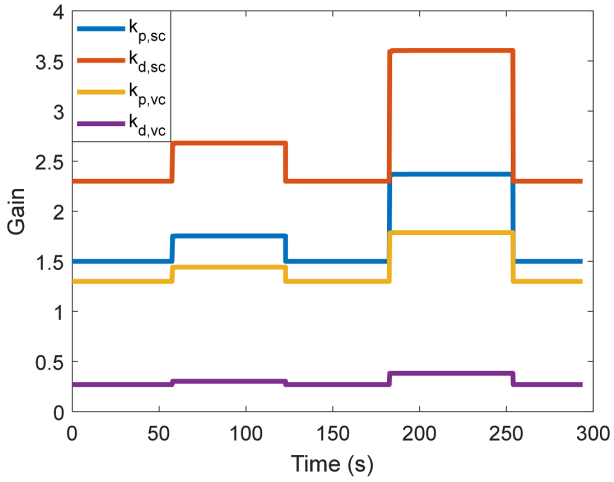

FIGURE 19. Evolution of controller gains.

beginning then moved with a constant velocity as big as 20 m/s. On the other hand, the host vehicle started with 0 m/s velocities so that the relative distance between the host vehicle and actor 3 is big, as shown in Figure 16. As a result, the host vehicle was in CC mode initially and changed after a few seconds into spacing control mode to maintain a safe distance. Around 160 seconds, the host vehicle decelerated to 0 m/s due to its arrival at the passenger's location and ready to carry passengers to another location.

d: PHASE 4

Again, after picking up passengers, the vehicle's mass changed to 2950 kg, and the vehicle in front of the host vehicle changed to actor 4. In this phase, the host vehicle and actor 4 have the same velocity at the beginning, as big as 0 m/s, and separate as far as 25 meters, as shown in Figure 15 and Figure 16. In this phase, the host vehicle is fully in spacing control mode. Actor 4 performs more often acceleration and deceleration than previous actors. We can observe that the host vehicle is able to maintain a safe distance, as shown in Figure 16. However, there is a small magnitude (red circle) when actor 4 does hard braking. It is because the vehicle with ACC system using a time gap 1 second. The time gap 1 second in this work is too small and makes velocity oscillation when the preceding vehicle does hard braking. Commonly, time gap for vehicle ACC-based in range 1-2 seconds. Hence, add more time gaps can solve this issue. Another way, we can use the CACC system where it only requires a small time gap of less than 1 second albeit needs a communication device to communicate with other vehicles. At around 240 seconds, the host vehicle decelerated to 0 m/s due to its arrival at passenger's destination and ready to pick up other passengers.

e: PHASE 5

In this phase, the host vehicle performs similar to phases 1 and 3.

Overall, Figure 15 and Figure 16 show that our switching strategy, as defined in (40), successfully generates a smooth transition between CC and spacing control mode. Figure 17 shows the evolution distance error. We can observe that distance error converges close to zero during spacing control mode. The legend $e_{sc,1}$ in Figure 17 can be calculated using equation (4) respect to actor 1.

Figure 18 shows the vehicle's mass estimation and the error estimation. The RLS with the forgetting factor algorithm succeeds in estimating the vehicle's mass with small error estimation and time convergence when the vehicle's mass is changed. Figure 19 shows the evolution of controller gains. The controller gains adaptively changed based on the vehicle's mass during ACC operation.

Remark 8: We stated again that this work is not concentrated on vehicle mass estimation. We focused on developing the ACC controller using the gain scheduling technique and analyzed the controller robustness under the LPV system. The vehicle's mass estimation is required because we assumed that the vehicle's mass varied during ACC operation. Further

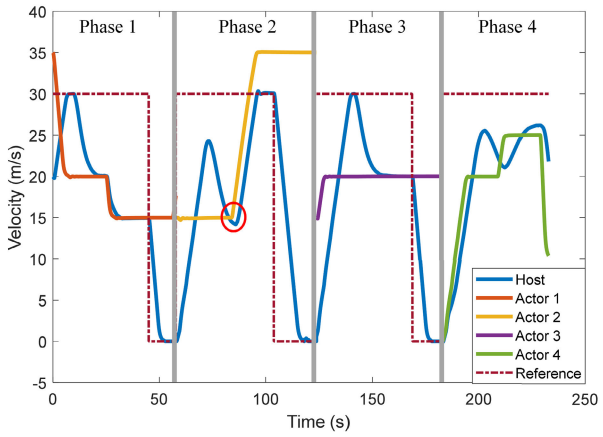

FIGURE 20. Velocity of the host vehicle using fixed controller gains.

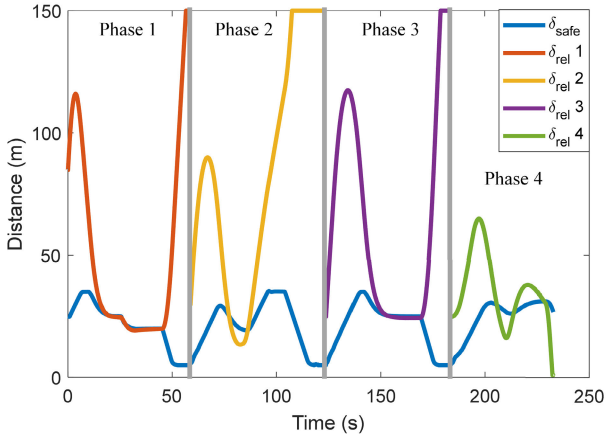

FIGURE 21. Distance tracking of the host vehicle using fixed controller gains.

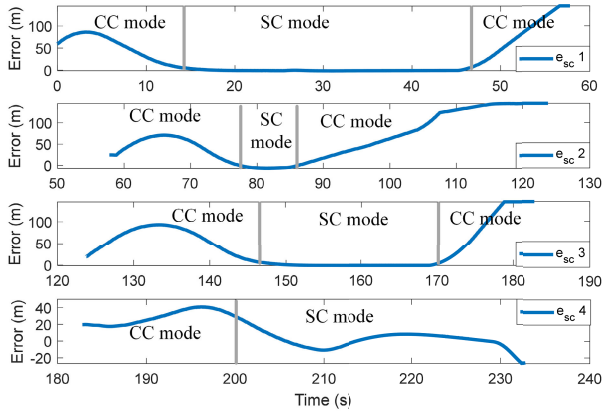

FIGURE 22. Evolution distance error of the host vehicle using fixed controller gains.

detail about the vehicle's mass estimation can be referred to in [59], [60].

Remark 9: In this paper, the RLS with the forgetting factor is used to estimate the vehicle's mass. In Figure 15, the vehicle will stop to pick up or drop passengers. In this period, we reinitialized the estimation algorithm to improve the estimation accuracy and convergence time.

2) ACC WITH FIXED PD CONTROLLER GAIN

Herein, the fixed controller gains are set as shown in Table 3 when the vehicle's mass is 1820 kg (without passenger). As a result, Phase 1 and Phase 3 in Figure 20 will show similar to Phase 1 and Phase 3 in Figure 15. However, Phase 2 and Phase 4 will be completely different due to the vehicle's mass being changed.

a: PHASE 2

After picked up passengers, the vehicle's mass changed to 2150 kg. The vehicle in front of the host vehicle changed to be actor 2. The host vehicle was in the spacing control mode, then changed into CC mode when actor 2 accelerated. It seems all things are similar to Phase 2 using gain scheduling. However, Figure 21 show the performance tracking when the host vehicle in spacing control mode degraded (red circle) compared Figure 16. The error is around 7 meters, as shown in Figure 22. The negative sign in Figure 22 indicates that relative distance is smaller than safe distance. This behavior leads to host vehicles having crash possibilities with other vehicles. At around 104 seconds, the host vehicle decelerated to 0 m/s due to its arrival at passenger's destination and ready to pick up other passengers.

b: PHASE 4

The vehicle's mass changed far from the nominal (without passenger) to be 2950 kg, and the vehicle in front of the host vehicle changed to be actor 4. Figure 21 show that the host vehicle has poor tracking performance and leads to crash with actor 4. It is proven in Figure 21 where $\delta_{sc,4}$ value is zero. Figure 22 show the $e_{sc,4}$ value is less than zero which is violated the spacing control mode objective as defined in (4).

Both ACC simulations for different controller settings such as PD gain scheduling and fixed PD controller gain are done by the same treatment including scenario, sensor settings, and simulation settings. The only difference is the controller gain on PD gain scheduling varied depend on the vehicle's mass during the ACC operation. Conversely, fixed PD controller gain used fixed nominal controller gain at vehicle's mass 1820 kg during the ACC operation. The host vehicle with PD gain scheduling has not degraded performance under different vehicle's mass for both ACC modes. However, the contrast results are shown by the host vehicle with fixed PD controller gain where the host vehicle has crashed with actor 4 in phase 4. Moreover, the simulation confirmed that the host vehicle with PD gain scheduling can handle larger uncertainty than the fixed PD gain controller. It appropriated with robustness analysis, either disk margin or worst-case gain, that confirmed controller gain is robust for several frozen points and vehicle's mass rate changes.

VI. CONCLUSION

This paper focuses on the passenger vehicle type that operates like a self-driving taxi with ACC features under varying

vehicle mass. As a result, the LPV system is adopted instead of the LTI system. The simulation is done by joint PreScan with Matlab/Simulink. PreScan provided the highly nonlinear vehicle, scenario, and sensor model while control algorithm, decision making, and target tracking are built in Matlab/Simulink. Due to the LPV system based on the linear model which then an identification method is utilized. A PD gain scheduling is designed based on those linear models. After that, disk margin is used to analyze the stability margin of the LPV system at each frozen point. Moreover, the robust performance margin of the LPV system is measured by the worst-case gain where the uncertainty is modeled by IQC. The superior performance of PD gain scheduling is shown by comparing it to PD fixed-gain controller through simulation. In the future, we will investigate and analyze the vehicle with cooperative-ACC feature under varying time gaps and vehicle mass with addressed the string stability criteria.

REFERENCES

[1] P. Warrendale, *Taxonomy and Definitions for Terms Related to Driving Automation Systems for On-Road Motor Vehicles*. Warrendale, PA, USA: Society of Automotive Engineers. Accessed: May 1, 2021. [Online]. Available: https://www.sae.org/standards/content/j3016_201806/

[2] M. R. Hidavatullah, J.-C. Juang, Z.-H. Fang, and W.-H. Chang, "Heterogeneous platooning vehicle with robust sensor fault detection and estimation," in *Proc. Int. Symp. Comput., Consum. Control (IS3C)*, Nov. 2020, pp. 436–439.

[3] E. Rasool, M. Liaquat, A. I. Bhatti, and A. Mehmood, "Cooperative adaptive cruise control with fuel efficiency using PMP technique," in *Proc. 5th Int. Conf. Control, Autom. Robot. (ICCAR)*, Apr. 2019, pp. 396–400.

[4] L. Xiao, M. Wang, W. Schakel, and B. van Arem, "Unravelling effects of cooperative adaptive cruise control deactivation on traffic flow characteristics at merging bottlenecks," *Transp. Res. C, Emerg. Technol.*, vol. 96, pp. 380–397, Nov. 2018.

[5] M. Makridis, K. Mattas, and B. Ciuffo, "Response time and time headway of an adaptive cruise control. An empirical characterization and potential impacts on road capacity," *IEEE Trans. Intell. Transp. Syst.*, vol. 21, no. 4, pp. 1677–1686, Apr. 2020.

[6] E. Alcala, V. Puig, J. Quevedo, and T. Escobet, "Gain-scheduling LPV control for autonomous vehicles including friction force estimation and compensation mechanism," *IET Control Theory Appl.*, vol. 12, no. 12, pp. 1683–1693, Aug. 2018.

[7] W. Zong, C. Zhang, Z. Wang, J. Zhu, and Q. Chen, "Architecture design and implementation of an autonomous vehicle," *IEEE Access*, vol. 6, pp. 21956–21970, 2018.

[8] C. Vilas Samak, T. Vilas Samak, and S. Kandhasamy, "Control strategies for autonomous vehicles," 2020, *arXiv:2011.08729*. [Online]. Available: http://arxiv.org/abs/2011.08729

[9] R. Rajamani, *Vehicle Dynamics and Control*, 2nd ed. New York, NY, USA: Springer, 2011.

[10] S. Wang, Y. Hui, X. Sun, and D. Shi, "Neural network sliding mode control of intelligent vehicle longitudinal dynamics," *IEEE Access*, vol. 7, pp. 162333–162342, 2019.

[11] Y. Sun, J. Xu, G. Lin, W. Ji, and L. Wang, "RBF neural network-based supervisor control for maglev vehicles on an elastic track with network time delay," *IEEE Trans. Ind. Informat.*, vol. 18, no. 1, pp. 509–519, Jan. 2022.

[12] Y. Sun, J. Xu, H. Wu, G. Lin, and S. Mumtaz, "Deep learning based semi-supervised control for vertical security of maglev vehicle with guaranteed bounded airgap," *IEEE Trans. Intell. Transp. Syst.*, vol. 22, no. 7, pp. 4431–4442, Jul. 2021.

[13] X. Lin and D. Gorges, "Robust model predictive control of linear systems with predictable disturbance with application to multiobjective adaptive cruise control," *IEEE Trans. Control Syst. Technol.*, vol. 28, no. 4, pp. 1460–1475, Jul. 2020.

[14] A. Wasserburger, A. Schirrer, N. Didcock, and C. Hametner, "A probability-based short-term velocity prediction method for energy-efficient cruise control," *IEEE Trans. Veh. Technol.*, vol. 69, no. 12, pp. 14424–14435, Dec. 2020.

[15] B. Sakhdari and N. L. Azad, "Adaptive tube-based nonlinear MPC for economic autonomous cruise control of plug-in hybrid electric vehicles," *IEEE Trans. Veh. Technol.*, vol. 67, no. 12, pp. 11390–11401, Dec. 2018.

[16] S. E. Li, Z. Jia, K. Li, and B. Cheng, "Fast online computation of a model predictive controller and its application to fuel economy-oriented adaptive cruise control," *IEEE Trans. Intell. Transp. Syst.*, vol. 16, no. 3, pp. 1199–1209, Jun. 2015.

[17] S. E. Li, Q. Guo, S. Xu, J. Duan, S. Li, C. Li, and K. Su, "Performance enhanced predictive control for adaptive cruise control system considering road elevation information," *IEEE Trans. Intell. Veh.*, vol. 2, no. 3, pp. 150–160, Sep. 2017.

[18] M. M. Brugnolli, B. A. Angelico, and A. A. M. Lagana, "Predictive adaptive cruise control using a customized ECU," *IEEE Access*, vol. 7, pp. 55305–55317, 2019.

[19] J. Jiang, F. Ding, Y. Zhou, J. Wu, and H. Tan, "A personalized human Drivers' risk sensitive characteristics depicting stochastic optimal control algorithm for adaptive cruise control," *IEEE Access*, vol. 8, pp. 145056–145066, 2020.

[20] N. Bekiaris-Liberis, C. Roncoli, and M. Papageorgiou, "Predictor-based adaptive cruise control design," *IEEE Trans. Intell. Transp. Syst.*, vol. 19, no. 10, pp. 3181–3195, Oct. 2018.

[21] N. Bekiaris-Liberis and A. I. Delis, "PDE-based feedback control of freeway traffic flow via time-gap manipulation of ACC-equipped vehicles," *IEEE Trans. Control Syst. Technol.*, vol. 29, no. 1, pp. 461–469, Jan. 2021.

[22] C. Wu, Z. Xu, Y. Liu, C. Fu, K. Li, and M. Hu, "Spacing policies for adaptive cruise control: A survey," *IEEE Access*, vol. 8, pp. 50149–50162, 2020.

[23] L. Yang, J. Mao, K. Liu, J. Du, and J. Liu, "An adaptive cruise control method based on improved variable time headway strategy and particle swarm optimization algorithm," *IEEE Access*, vol. 8, pp. 168333–168343, 2020.

[24] X. Chen, J. Yang, C. Zhai, J. Lou, and C. Yan, "Economic adaptive cruise control for electric vehicles based on ADHDP in a car-following scenario," *IEEE Access*, vol. 9, pp. 74949–74958, 2021.

[25] H. Liu, C. Miao, and G. G. Zhu, "Economic adaptive cruise control for a power split hybrid electric vehicle," *IEEE Trans. Intell. Transp. Syst.*, vol. 21, no. 10, pp. 4161–4170, Oct. 2020.

[26] G. Li and D. Görges, "Ecological adaptive cruise control for vehicles with step-gear transmission based on reinforcement learning," *IEEE Trans. Intell. Transp. Syst.*, vol. 21, no. 11, pp. 4895–4905, Nov. 2019.

[27] Y. Jia, R. Jibrin, and D. Gorges, "Energy-optimal adaptive cruise control for electric vehicles based on linear and nonlinear model predictive control," *IEEE Trans. Veh. Technol.*, vol. 69, no. 12, pp. 14173–14187, Dec. 2020.

[28] C. Lu, J. Dong, L. Hu, and C. Liu, "An ecological adaptive cruise control for mixed traffic and its stabilization effect," *IEEE Access*, vol. 7, pp. 81246–81256, 2019.

[29] S. Tajeddin, S. Ekhtiari, M. Faieghi, and N. L. Azad, "Ecological adaptive cruise control with optimal lane selection in connected vehicle environments," *IEEE Trans. Intell. Transp. Syst.*, vol. 21, no. 11, pp. 4538–4549, Nov. 2020.

[30] H. Chen, L. L. Guo, and H. T. Ding, "Real-time predictive cruise control for eco-driving taking into account traffic constraints," *IEEE Trans. Intell. Transp. Syst.*, vol. 20, no. 8, pp. 2858–2868, Aug. 2019.

[31] S. E. Li, Q. Guo, L. Xin, B. Cheng, and K. Li, "Fuel-saving servo-loop control for an adaptive cruise control system of road vehicles with step-gear transmission," *IEEE Trans. Veh. Technol.*, vol. 66, no. 3, pp. 2033–2043, Mar. 2017.

[32] G. Li and D. Görges, "Ecological adaptive cruise control and energy management strategy for hybrid electric vehicles based on heuristic dynamic programming," *IEEE Trans. Intell. Transp. Syst.*, vol. 20, no. 9, pp. 3526–3535, Sep. 2019.

[33] R. Dang, J. Wang, S. E. Li, and K. Li, "Coordinated adaptive cruise control system with lane-change assistance," *IEEE Trans. Intell. Transp. Syst.*, vol. 16, no. 5, pp. 2373–2383, Oct. 2015.

[34] X. Xu, J. W. Grizzle, P. Tabuada, and A. D. Ames, "Correctness guarantees for the composition of lane keeping and adaptive cruise control," *IEEE Trans. Autom. Sci. Eng.* , vol. 15, no. 3, pp. 1216–1229, Jul. 2018.

[35] J. Huang, Y. Chen, X. Peng, L. Hu, and D. Cao, "Study on the driving style adaptive vehicle longitudinal control strategy," *IEEE/CAA J. Automatica Sinica*, vol. 7, no. 4, pp. 1107–1115, Jul. 2020.
[36] J. Lunze, "Adaptive cruise control with guaranteed collision avoidance," *IEEE Trans. Intell. Transp. Syst.*, vol. 20, no. 5, pp. 1897–1907, May 2019.
[37] M. G. Plessen, D. Bernardini, H. Esen, and A. Bemporad, "Spatial-based predictive control and geometric corridor planning for adaptive cruise control coupled with obstacle avoidance," *IEEE Trans. Control Syst. Technol.*, vol. 26, no. 1, pp. 38–50, Jan. 2018.
[38] S. Cheng, L. Li, M.-M. Mei, Y.-L. Nie, and L. Zhao, "Multiple-objective adaptive cruise control system integrated with DYC," *IEEE Trans. Veh. Technol.*, vol. 68, no. 5, pp. 4550–4559, May 2019.
[39] Z. Li, T. Chu, I. V. Kolmanovsky, and X. Yin, "Training drift counteraction optimal control policies using reinforcement learning: An adaptive cruise control example," *IEEE Trans. Intell. Transp. Syst.*, vol. 19, no. 9, pp. 2903–2912, Sep. 2018.
[40] W. Gao, J. Gao, K. Ozbay, and Z.-P. Jiang, "Reinforcement-learning-based cooperative adaptive cruise control of buses in the Lincoln tunnel corridor with time-varying topology," *IEEE Trans. Intell. Transp. Syst.*, vol. 20, no. 10, pp. 3796–3805, Oct. 2019.
[41] H. Kazemi, H. N. Mahjoub, A. Tahmasbi-Sarvestani, and Y. P. Fallah, "A learning-based stochastic MPC design for cooperative adaptive cruise control to handle interfering vehicles," *IEEE Trans. Intell. Veh.*, vol. 3, no. 3, pp. 266–275, Sep. 2018.
[42] J. Chen, G. Yu, and X. Yan, "Data based parameter setting method for adaptive cruise control," *IEEE Access*, vol. 8, pp. 15291–15302, 2020.
[43] A. P. Bolduc, L. Guo, and Y. Jia, "Multimodel approach to personalized autonomous adaptive cruise control," *IEEE Trans. Intell. Vehicles*, vol. 4, no. 2, pp. 321–330, Jun. 2019.
[44] G. Gunter, C. Janssen, W. Barbour, R. E. Stern, and D. B. Work, "Model-based string stability of adaptive cruise control systems using field data," *IEEE Trans. Intell. Veh.*, vol. 5, no. 1, pp. 90–99, Mar. 2020.
[45] B. Németh, P. Gáspár, R. Orjuela, and M. Basset, "LPV-based control design of an adaptive cruise control system for road vehicles," *IFAC-PapersOnLine*, vol. 48, no. 14, pp. 62–67, 2015.
[46] H. Basargan, A. Mihály, P. Gáspár, and O. Sename, "Adaptive semi-active suspension and cruise control through LPV technique," *Appl. Sci.*, vol. 11, no. 1, p. 290, Dec. 2020.
[47] G. Q. B. Tran, T.-P. Pham, O. Sename, E. Costa, and P. Gaspar, "Integrated comfort-adaptive cruise and semi-active suspension control for an autonomous vehicle: An LPV approach," *Electronics*, vol. 10, no. 7, p. 813, Mar. 2021.
[48] E. Alcalá, V. Puig, and J. Quevedo, "LPV-MPC control for autonomous vehicles," *IFAC-PapersOnLine*, vol. 52, no. 28, pp. 106–113, 2019.
[49] J. Lan, D. Zhao, and D. Tian, "Robust cooperative adaptive cruise control of vehicles on banked and curved roads with sensor bias," in *Proc. Amer. Control Conf. (ACC)*, Jul. 2020, pp. 2276–2281.
[50] K. Laib, O. Sename, and L. Dugard, "String stable H_∞ LPV cooperative adaptive cruise control with a variable time headway," *IFAC-Papers Line*, vol. 53, no. 2, pp. 15140–15145, 2020.
[51] A.-K. Schug, P. Seiler, and H. Pfifer, "Robustness margins for linear parameter varying systems," *Aerosp. Lab*, no. 13, pp, pp. 1–9, Jun. 2017.
[52] H. Pfifer and P. Seiler, "Robustness analysis of linear parameter varying systems using integral quadratic constraints," *Int. J. Robust Nonlinear Control*, vol. 25, no. 15, pp. 2843–2864, 2014.
[53] *PreScan User Manual Version 8.5.0.*, TASS International, Helmond, The Netherlands, 2018.
[54] M. R. Hidayatullah and J.-C. Juang, "Centralized and distributed control framework under homogeneous and heterogeneous platoon," *IEEE Access*, vol. 9, pp. 49629–49648, 2021.
[55] T. Yang, N. Sun, and Y. Fang, "Adaptive fuzzy control for a class of MIMO underactuated systems with plant uncertainties and actuator deadzones: Design and experiments," *IEEE Trans. Cybern.*, early access, Feb. 2, 2021, doi: 10.1109/TCYB.2021.3050475.
[56] H. Zhang, G. Zhang, and J. Wang, "$\mathcal{H}_\infty$ observer design for LPV systems with uncertain measurements on scheduling variables: Application to an electric ground vehicle," *IEEE/ASME Trans. Mechatronics*, vol. 21, no. 3, pp. 1659–1670, Jun. 2016.
[57] P. Li, A.-T. Nguyen, H. Du, Y. Wang, and H. Zhang, "Polytopic LPV approaches for intelligent automotive systems: State of the art and future challenges," *Mech. Syst. Signal Process.*, vol. 161, Dec. 2021, Art. no. 107931.
[58] K.-Z. Liu and Y. Yao, *Robust Control: Theory and Applications*. Hoboken, NJ, USA: Wiley, 2016.
[59] J. Ghosh, S. Foulard, and R. Fietzek, "Vehicle mass estimation from CAN data and drivetrain torque observer," SAE, Warrendale, PA, USA, Tech. Rep. 2017-01-1590, Mar. 2017, doi: 10.4271/2017-01-1590.
[60] D. Zhang, A. Ivanco, and Z. Filipi, "Model-based estimation of vehicle aerodynamic drag and rolling resistance," *SAE Int. J. Commercial Veh.*, vol. 8, no. 2, pp. 433–439, Sep. 2015.
[61] P. Seiler, A. Packard, and P. Gahinet, "An introduction to disk margins," *IEEE Control Syst. Mag.*, vol. 40, no. 5, pp. 78–95, Sep. 2020.
[62] Y. Zhu, H. He, and D. Zhao, "LMI-based synthesis of string-stable controller for cooperative adaptive cruise control," *IEEE Trans. Intell. Transp. Syst.*, vol. 21, no. 11, pp. 4516–4525, Nov. 2020.

MUHAMMAD RONY HIDAYATULLAH was born in Mangkayahu, South Kalimantan, Indonesia, in 1997. He received the B.S. degree in electrical engineering, focusing on control engineering, from the University of Brawijaya, Malang, Indonesia, in 2017, and the M.S. degree in electrical engineering from National Cheng Kung University, Tainan, Taiwan, in 2019, where he is currently pursuing the Ph.D. degree in electrical engineering.

His research interests include the string stability analysis of platooning vehicle, multi-agent control, autonomous driving control, and sensor fusion.

JYH-CHING JUANG (Member, IEEE) received the B.S. degree in control engineering and the M.S. degree in electronics from National Chiao Tung University, Hsinchu, Taiwan, in 1980 and 1982, respectively, and the Ph.D. degree in electrical engineering from the University of Southern California, Los Angeles, CA, USA, in 1987.

He was with Lockheed Martin Aeronautics Company, Burbank, CA, before he joined the Department of Electrical Engineering, National Cheng Kung University, Tainan, Taiwan, as a Faculty Member, in 1993, where he is currently a Professor. Recently, he is also the Head of Taiwan CAR Lab. His research interests include robust control, global navigation satellite systems (GNSSs) signal processing, GNSS reflectometry, sensor fusion, and autonomous driving.